Exhibit A

Biophysical Journal Volume 91 August 2006 1441–1451

Time-Resolved Microspectroscopy on a Single Crystal of Bacteriorhodopsin Reveals Lattice-Induced Differences in the Photocycle Kinetics

R. Efremov,*† V. I. Gordeliy,*† J. Heberle,*‡ and G. Büldt*

*Forschungszentrum Jülich, IBI-2: Structural Biology, 52425 Jülich, Germany; †Centre of Biophysics and Physical Chemistry of Supramolecular Structures, Moscow Institute of Physics and Technology, 141700 Dolgoprudny, Russia; and ‡University of Bielefeld, Biophysical Chemistry (PC III), 33615 Bielefeld, Germany

ABSTRACT The determination of the intermediate state structures of the bacteriorhodopsin photocycle has lead to an unprecedented level of understanding of the catalytic process exerted by a membrane protein. However, the crystallographic structures of the intermediate states are only relevant if the working cycle is not impaired by the crystal lattice. Therefore, we applied visible and Fourier transform infrared spectroscopy (FTIR) microspectroscopy with microsecond time resolution to compare the photoreaction of a single bacteriorhodopsin crystal to that of bacteriorhodopsin residing in the native purple membrane. The analysis of the FTIR difference spectra of the resolved intermediate states reveals great similarity in structural changes taking place in the crystal and in PM. However, the kinetics of the photocycle are significantly altered in the three-dimensional crystal as compared to PM. Strikingly, the L state decay is accelerated in the crystal, whereas the M decay is delayed. The physical origin of this deviation and the implications for trapping of intermediate states are discussed. As a methodological advance, time-resolved step-scan FTIR spectroscopy on a single protein crystal is demonstrated for the first time which may be used in the future to gauge the functionality of other crystallized proteins with the molecular resolution of vibrational spectroscopy.

INTRODUCTION

The elucidation of the molecular mechanism of energy conversion by living organisms is of particular interest to biophysics. One of the most intensively studied but still controversially discussed primary energy converter is bacteriorhodopsin (bR). bR is a 27-kDa integral membrane protein from the halophilic archaea *Halobacterium salinarum* (1). It is the simplest known proton pump. As cofactor, bR contains *all-trans* retinal covalently linked to Lys-216 via a protonated Schiff base (SB). Photon absorption induces the working cycle of the protein (photocycle). The first atomic motion leads to *13-cis* isomerization of the retinal, which is eventually followed by a sequence of proton transfer reactions that finally result in positive charge transfer out of the cell (2,3).

The development of new crystallization procedures (4–7) resulted in well-ordered three-dimensional (3D) crystals that allowed us to solve the bR structure to high resolution. The next step in high-resolution crystallographic studies was the determination of the structural changes that accompany the photocycle (8). Most of the intermediate state structures have been solved from crystals of space group $P6_3$ grown in lipidic cubic phase (4). The packing of molecules in this crystal form is similar to the natural two-dimensional crystals (purple membrane; PM) (9). These crystals diffract to the highest resolution (10). The crystallized bR molecules were shown to be fully functional; that is, the crystals were investigated by resonance Raman and time-resolved (TR) Fourier transform infrared spectroscopy (FTIR) spectroscopy in millisecond range, and it was concluded that retinal isomerization, conformational changes of the protein backbone, and proton translocation steps proceed virtually indistinguishable from those in the native membranes (11). Later it turned out that the procedures developed to trap intermediate states of bR in PM (12) are not rigorously applicable to bR in crystals (13,14). Moreover, it was suggested that lipidic cubic phase crystallization results in internally dehydrated bR crystals (15). These contradictions were the motivation for the more thorough investigation of the photochemical properties of bR in crystals.

The major limiting factor in spectroscopic studies of protein crystals is their small size, which usually does not exceed a few hundred microns. However, when a structure of an intermediate of a light-sensitive protein is the focus of a crystallographic study, it is prerequisite to characterize photoproduct by spectroscopic methods. The most common technique is stationary visible absorbance spectroscopy (16–18). Among more sophisticated methods are TR visible absorbance spectroscopy (19–21) and static FTIR spectroscopy (22,23). Another obstacle for a spectroscopic study is to obtain crystals with the suitable shape. Special approaches like crystallization in capillary (19) or between parallel glass plates (22) were used in some cases. Under our conditions, bR crystallizes in the form of thin hexagonal plates, which are naturally suitable for spectroscopic studies.

We were able to demonstrate in previous FTIR spectroscopic experiments that bR is fully functional in 3D crystals (11). However, kinetic details could not be studied due to the

Submitted February 14, 2006, and accepted for publication May 16, 2006.

Address reprint requests to J. Heberle, Tel.: 49-0521-106-2055; Fax: 49-0521-106-2981; E-mail: joachim.heberle@uni-bielefeld.de.

0006-3495/06/08/1441/11 $2.00

doi: 10.1529/biophysj.106.083345

poor time resolution of rapid-scan FTIR (millisecond range). Moreover, previous work was performed on an ensemble of crystals. In this study, we applied visible and FTIR microspectroscopy with microsecond time resolution to compare the photocycles of a single bR crystal to that of PMs under conditions commonly used in crystallography. It is found that bR undergoes transformations via the intermediate states L, M, N, and O in the crystal. The detailed comparison of the FTIR difference spectra of the resolved intermediate states reveals great similarity in structural changes taking place in crystals and PM. However, the kinetics of the photocycle is significantly altered in 3D crystals as compared to PM.

MATERIAL AND METHODS

Purple membrane preparation and bR crystallization

PMs were isolated from *H. salinarum* strain S9 (24). For crystallization, bR was solubilized in β-octylglycopyranoside (OG). Crystals were grown in the cubic phase of monoolein (1-oleoyl-*rac*-glycerol, MO, NU-Chek Prep, Elysian, MN) (4) as described (25). Crystals were separated from the lipidic cubic phase by dissolving the lysolipid in 2 ml of an aqueous solution of 3 M NaH_2PO_4/Na_2HPO_4 (pH 5.6) buffer in the presence of OG.

Sample preparation for spectroscopy

Spectroscopic measurements in the visible wavelength range were performed in a horizontal glass cuvette with two circular cover glasses separated by a plastic spacer. A bR crystal adhered on the bottom window of the cuvette was overlaid with 200 μl of 3 M Na-Pi pH 5.6 buffer and sealed with another window using vacuum grease. For comparison, a dried film of PM has been rehydrated in the same way.

For infrared measurements, crystals were placed in the center of a BaF_2 window using a cryoloop overlaid with 10 μl of 3 M phosphate buffer (pH 5.6) and sealed with a second BaF_2 window using vacuum grease. Care was taken to avoid mechanical destruction of the bR crystals. Only crystals with optimal thickness (optical density ~ 0.7 at 570 nm) were selected. The diameter of the sampling field of the microscope was limited to 180–250 μm by an aperture wheel. For comparison, PM was dried on a BaF_2 window, covered by 100 μl of phosphate buffer (see above) and equilibrated for >3 h. Finally, excess buffer was removed and the sample sealed. For measurements in D_2O, 3 M deuterated phosphate buffer was prepared from the protonated buffer by several successive lyophilization steps. Crystals were soaked overnight in deuterated buffer before the spectroscopic experiments. Hydrogen/deuterium (H/D) exchange in PM was achieved by several successive washings steps of the film with deuterated buffer and 2 h of equilibration after each wash. The residual H_2O content in the samples was <5% as judged from the absorbance at 3400 cm^{-1} (O-H stretching vibration) and 2500 cm^{-1} (O-D stretch).

Experimental setup for time-resolved microspectroscopy

A schematic block diagram of the experimental setup is shown in Fig. 1 *a*. The principal part of the setup is a Cassegrain-type microscope (focusing mirrors only). A single crystal was placed in the focal plane (Fig. 1 *b*). The microscope can be operated in three different modes. In UV-Vis mode, one of the oculars of the microscope is coupled via a quartz fiber bundle to a spectrograph (Acton Research, Acton, MA) with an intensified charge-coupled device (CCD) camera (CCD-576G, Princeton Instruments, Monmouth Junction, NJ) as detector. The emission from a continuous Xe-lamp is used as probe light. Time-gated difference spectra with a time resolution of 10 ns can also be acquired with the intensified CCD camera. However, the intense white probe light leads to the accumulation of photoproducts. Therefore, experiments at single wavelength are preferred. A home-built flash photolysis setup was constructed which employs interference filters (half-width <10 nm) that are placed between the Xe-lamp and the sample. For pulsed excitation, the pulsed emission of a frequency-doubled Nd:YAG laser (532 nm, 8 ns, 3 mJ/cm^2) was used. A notch filter (OD 6 at 532 nm, Kaiser Optical Systems, Ann Arbor, MI) was placed in front of the photomultiplier (R3788, Hamamatsu, Herrsching, Germany) to block scattered laser light. The signal from the transmitted light was amplified with a home-built amplifier (1-μs response time) and fed into a digital oscilloscope (Hewlett Packard, Palo Alto, CA; 54510A, 250 MHz, 8000 points, GPIB interface) to detect transient absorbance changes in the time range between 10 μs and 1 s. Data from 1536 laser flashes were averaged at each wavelength to improve the signal/noise ratio.

In infrared (IR) mode, the modulated emission from the globar of the IFS66v spectrometer (Bruker, Billerica, MA) is focused by the microscope on the sample. The transmitted light is focused on the mercury cadmium telluride (MCT) detector of the microscope. The signal from the detector is coupled to a preamplifier (analog bandwidth 40 kHz) operating in alternating current for steady-state measurements or direct current output mode for step-scan experiments. The photocycle was excited with a repetition frequency of 5.9 and 4.0 Hz for PM and crystal, respectively. Step-scan data were recorded using a sequence of 942 time points distributed uniformly on a logarithmic timescale between 7 μs and 160 ms. The sequence was generated by a programmable waveform generator (Wavetek model 39, Ismaning, Germany) that triggers data acquisition of the FTIR spectrometer. With a broadband interference filter (Optical Coating Laboratory, Santa Rosa, CA) limiting the free spectral range from 1900 to 1000 cm^{-1}, data were collected at 844 positions of the moving mirror of the interferometer corresponding to an optical resolution of 4.5 cm^{-1}. Data from 5 or 10 flashes were averaged at each mirror position, and 10–25 of such measurements were collected on each bR crystal. Finally, the data collected from two crystals were averaged for measurements in H_2O and from four crystals in D_2O. All experiments have been carried out at 20°C.

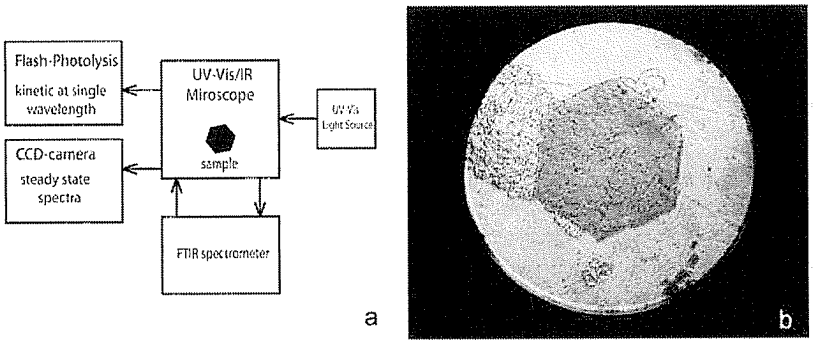

FIGURE 1 (*a*) Block diagram of the spectroscopic setup to perform TR UV/Vis and FTIR on a single protein microcrystal. (*b*) Hexagonal bR crystal imaged via the ocular of the microscope. Traces from the lipidic cubic phase used for crystallization appear at the left of the crystal as a transparent inhomogeneous paste.

Laser pulse intensity was optimized to minimize photobleaching, which resulted in the pulse power of ~3 mJ/cm^2. In addition, it was checked that the bR crystal preserves the diffraction properties (see Figs. S3 and S4) and hence crystallinity after illumination with 10^5 laser flashes.

To measure the light minus dark adapted spectrum, the 512 reference spectra were taken from samples that had been left in the dark overnight. After 1-min illumination with white light from the focused emission of the Xe-lamp, the 512 FTIR spectra were measured and the difference was calculated. Subsequent illumination did not increase the amplitude of the difference signal, confirming that complete light adaptation was achieved.

Data analysis

Global exponential fitting was applied to the TR data. Weights and number of essential exponentials were determined essentially as described by Müller et al. (26). Presented differential spectra were derived from a unidirectional kinetic model of the photocycle without branching (27).

RESULTS

The UV-Vis absorption spectrum of retinal proteins is very sensitive to the geometry of retinal and also to structural and electronic changes in the vicinity of the chromophore. This is exemplified by alterations in the chromophore absorption if bR is solubilized in detergent (28,29), if the protonation state of the SB or the adjacent aspartates is changed (30), or if the water content is reduced (31). It was reported that the absorption spectrum of bR crystal exhibits features of the partially dehydrated state of the protein (15).

Fig. 2 compares the absorbance spectra of bR residing in a single crystal and in the native PM, which have been recorded under the conditions used for x-ray crystallography (identical pH, salt, and temperature). Importantly, both samples were immersed in buffer providing equivalent conditions of hydration. It is evident that the spectral shapes of the retinal absorption (λ_{max} = 567 nm) are very similar. The deviations can be seen at lower wavelengths where the crystal shows higher absorbance than PM. The difference between the two spectra (Fig. 2 *b*) shows a monotonic decay which can be fitted to λ^{-4}. Hence, this difference can be attributed to stronger light scattering of the crystal, which is most probably caused by remainders of the lipidic cubic phase. Thus, the retinal absorption is the same for the crystal and PM under conditions used in crystallography before flash cooling of crystal. This is in agreement with the results of low temperature absorption spectroscopy reported by Royant et al. (14).

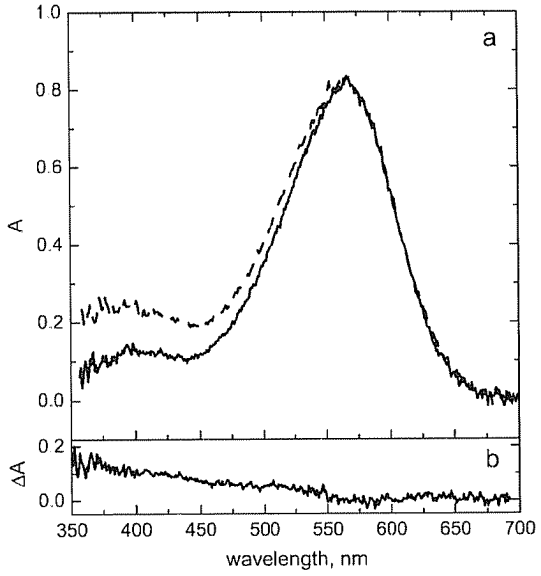

FIGURE 2 (*a*) Absorbance spectra of light-adapted PM (*solid line*) and crystal (*dashed line*). Spectra are scaled to match the absorbance at 570 nm. The data have been recorded at 20°C in 3 M Na-P$_i$ buffer (pH 5.6). The trace in panel (*b*) is the difference between the absorbance spectra of the crystal and PM.

Time-resolved UV-Vis experiments

The kinetics of the visible absorbance changes after pulsed excitation reflects the time evolution and the spectral characteristics of the intermediates during the course of the photocycle. Fig. 3 displays the photocycle kinetics of a single bR

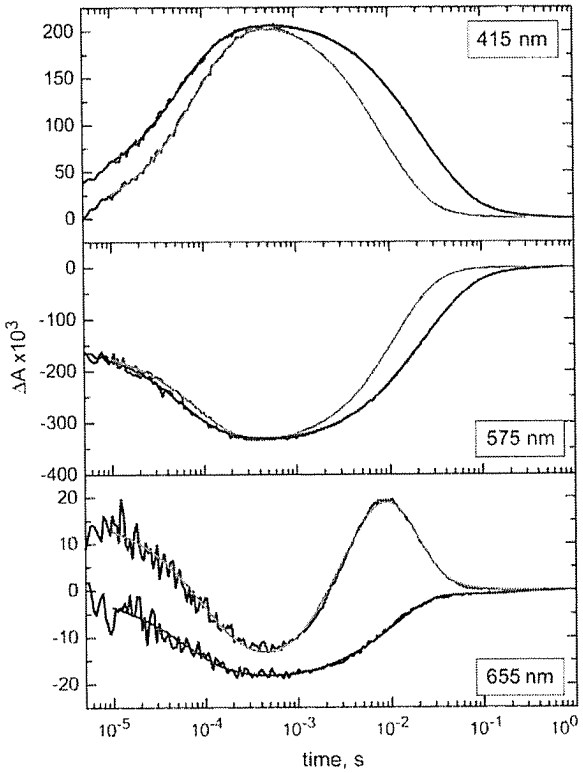

FIGURE 3 Transient absorbance changes at 415, 575, and 655 nm of PM and crystal. Experimental data are shown in black, and traces in green and blue represent fits of the data with the sum of five exponentials for PM and crystal, respectively. The two data sets have been scaled to match the amplitude of the absorbance changes. Experiments have been carried out in 3 M Na-P$_i$ (pH 5.6, 20°C).

crystal (*blue trace*) recorded from 10 μs to 1s. The kinetics of bR in PM has been taken under the same conditions and is also shown for comparison (*green trace*). The measurements have been performed at wavelengths that are characteristic for the rise and decay of specific intermediates. The M state kinetics has been recorded at 415 nm, the recovery of the ground state at 575 nm, and the O state at 655 nm. It can be seen in the top panel of Fig. 3 that the rise of the M intermediate is accelerated and the decay is delayed in the crystal as compared to PM. The transient appearance of the O intermediate is clearly detectable in the millisecond time domain for bR in PM (*green trace* in *bottom panel* of Fig. 3) but seemingly absent (see below) for bR in the 3D crystalline lattice (*blue trace*). The kinetic traces were analyzed by global exponential fitting. We found the sum of five exponentials is sufficient to adequately describe the kinetics of bR both in the crystal as well as in PM. The resulting time constants of the kinetics are presented in Table 1.

As a proton pump, bR exhibits kinetic isotope effects (KIE) when the protons are exchanged versus deuterons. Studies on PM showed that H_2O/D_2O exchange affects the rates of L→M and O→bR transitions (32,33). Indeed, the rise of the M intermediate in crystalline bR is retarded in D_2O by about fourfold (*green trace* in *top panel* of Fig. 4) as compared to the kinetics in H_2O (*blue trace*). Though the time constants of M rise change only by a factor of 2 (exps. 1 and 2 in Table 1), the corresponding equilibrium between L and M is shifted toward the L state for the fast and toward M for the slow time constant in D_2O. This increases the real deceleration of M rise to a factor of 4.

The M decay as well as the recovery of the ground state bR (*middle panel* in Fig. 4) shows no isotope effect. However, the equilibrium between M and O is shifted toward the O intermediate as a positive absorption band is detectable in D_2O at 655 nm (*green trace* in *bottom panel* of Fig. 4). Hence, the O state transiently accumulates under these conditions. As a matter of fact, the photocycle of crystalline bR includes the O intermediate, but the rate constants do not favor the transient accumulation in H_2O.

TABLE 1 Time constants of the kinetics of bR in PM and in the single crystal

No. of experiments	PM H_2O	Crystal	
		H_2O	D_2O
1	81 μs	53 μs	108 μs
2	320 μs	230 μs	480 μs
3	4.3 ms	10.7 ms	11.8 ms
4	10.2 ms	35 ms	36 ms
5	36 ms	170 ms	190 ms

Data have been recorded in the visible wavelength range. Experiments on the single crystal have been recorded in the presence of H_2O or D_2O, respectively (see Figs. 3 and 4 for the experimental data and the details on the sample conditions).

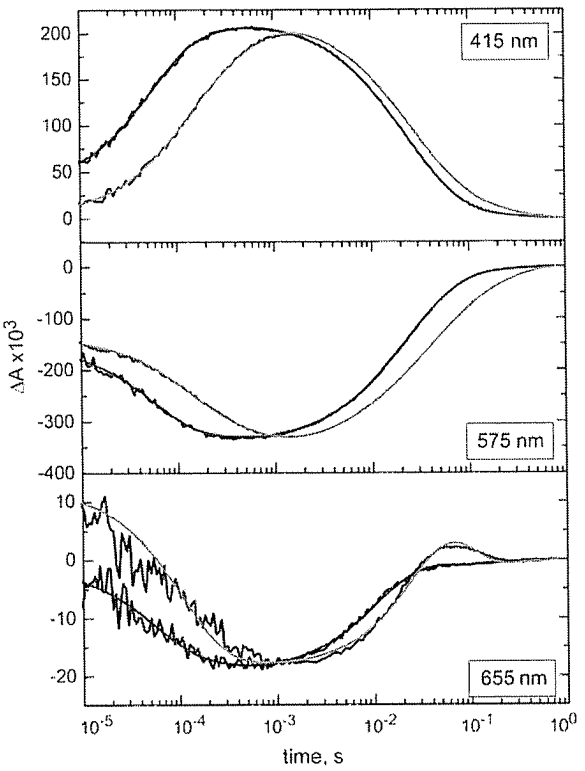

FIGURE 4 Transient absorbance changes at 415, 575, and 655 nm (from *top* to *bottom*) of a single bR crystal in D_2O (*green trace*). For comparison, the kinetics in the presence of H_2O (*blue trace*) are replotted from Fig. 3. The experimental data are shown in black, whereas the smooth green and blue traces represent fits to the data with the sum of five exponentials. The data are scaled to match the maximum absorbance change at each wavelength. Measurements have been carried out in 3 M Na-P_i pD at 20°C.

Light-dark adaptation

In the dark, the retinal chromophore of bR forms a thermal 1:1 equilibrium mixture of the *all-trans* and the *13-cis* isomers (34). Upon light adaptation, retinal is converted to the *all-trans* conformation (35). Dark/light adaptation in bR crystals is of particular interest for x-ray crystallography since incomplete light adaptation leads to a mixture of states which is difficult to take into account during data analysis. Fig. 5 shows FTIR difference spectra of light minus dark adapted PM (*black*) and crystal (*red*). Positive bands correspond to vibrations of light- and negative to dark-adapted bR.

All of the observed intensive bands have been assigned to chromophore vibrations. The frequency of the ethylenic vibration of retinal shifts from 1525 to 1539 cm^{-1} upon dark adaptation, which correlates with the blue shift of the bR absorbance spectrum. In the fingerprint region the C-C stretching vibrations at 1201 and 1169 cm^{-1} are characteristic of *all-trans* retinal, whereas the negative band at 1182 cm^{-1} corresponds to *13-cis* protonated retinal. The C=N stretch of the SB is observed at 1641 cm^{-1} in the light-adapted state. The bands at 1342 (−) and 1252 (+) cm^{-1} originate from the

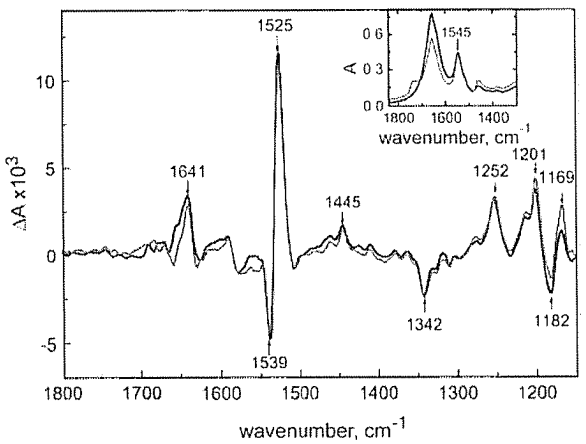

FIGURE 5 FTIR difference spectra of light minus dark adapted PM (*black*) and crystal (*red*). The frequencies of the most prominent bands are indicated and discussed in the text. Sample conditions are the same as in Fig. 2. The inset shows the scaled absorbance spectra of the samples in the amide I and II regions.

coupled N-H and C15-H in-plane bending vibrations of retinal in the dark- and light-adapted state, respectively (36). The band at 1445 cm^{-1} on the basis of the frequency can be tentatively assigned to asymmetric methyl deformation of retinal in the ground state.

It is evident that the spectra correspond well to each other and those reported earlier (37). The difference spectra have been scaled to match the intensity of the amide II bands (1545 cm^{-1}) in the absorbance spectra of the samples (see *inset* of Fig. 5). The intensity of the amide II band directly reflects the amount of probed protein, because it is not significantly overlapped with other than protein vibrations. Because the normalized difference spectra have equal amplitudes, the fractions of the molecules converted from the dark- to the light-adapted state are the same in PM and in the crystal. In conclusion, the similarity of the UV-Vis absorbance spectra of light-adapted PM and crystal as well as the identity of the FTIR difference spectra suggest that dark/light adaptation proceeds virtually identically in PM and the crystal, in qualitative and quantitative terms. Hence, the retinal in the bR crystal is quantitatively converted into the *all-trans* conformation by light adaptation.

Time-resolved FTIR spectroscopy in H_2O

To reveal the molecular details of the bR photocycle in a single crystal, TR step-scan FTIR spectroscopy has been performed. With this approach, the dynamics of protonation state change of key amino acids and of the retinal SB, conformational changes of the retinal as well as those of the protein backbone are determined and compared to those of bR residing in PM.

The sample conditions were chosen to closely match those used in x-ray crystallography before the crystal is frozen to 100 K (20°C, crystals immersed in 3 M Na-P_i buffer, pH 5.6). It is worthwhile to point out that the bR crystal does not lose crystallinity upon repetitive excitation by the Nd:YAG laser as gauged by recording diffraction patterns before and after the crystal was hit by 100,000 laser pulses (see Figs. S3 and S4 of the supplementary information). The absorbance changes were measured in the time range from 7 μs to 160 ms. Global exponential fitting was applied. As a consequence of the poorer signal/noise ratio of the TR FTIR data as compared to the ultraviolet/visible (UV/Vis) experiments, three exponentials were sufficient to fit the absorbance changes of the bR crystal. The resulting time constants are 30 μs, 13 ms, and 110 ms. Three exponential fittings of the photocycle kinetics of PM yielded time constants of 86 μs, 3.0 ms, and 16 ms. As already demonstrated by TR visible spectroscopy, the microsecond kinetics are faster in the crystal than in PM, whereas the millisecond kinetics are slower. This trend is maintained in D_2O (see below).

The spectra calculated from the unidirectional unbranched model of the photocycle are shown in Fig. 6. The spectra of PM (*black*) are overlaid with the corresponding spectra of crystal (*red*). The difference spectra corresponding to the earliest time constant (Fig. 6 *a*) look very similar for bR in the crystal or in PM. The spectra indicate the presence of a pure L state (36,38–40). The most intense band at 1525 cm^{-1} is assigned to the C=C stretch of retinal in the ground state. This band is shifted to 1550 cm^{-1} in the L state. Three negative bands at 1201 and 1169 arise from C-C stretching vibrations of the retinal in ground state bR. The positive band at 1190 cm^{-1} constitutes a fingerprint for the presence of

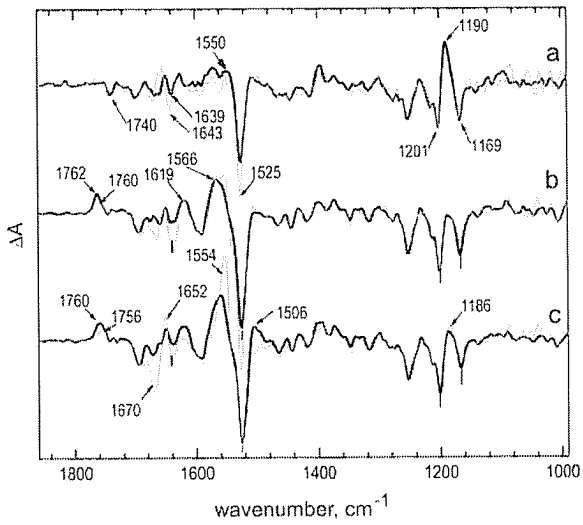

FIGURE 6 TR FTIR difference spectra of the bR derived from a unidirectional photocycle without branching. The spectra have been derived by globally fitting the IR kinetics with the sum of three exponentials. Black spectra correspond to the decay-associated difference spectra of bR in PM at time constants of 86 μs (*a*), 3.0 ms (*b*), and 16 ms (*c*). Spectra in red are the decay-associated difference spectra of bR in the single 3D crystal at time constants of 30 μs (*a*), 13 ms (*b*), and 110 ms (*c*).

13-cis retinal with a protonated SB. The frequency of C=N stretching vibrations of SB in bR are located at 1639 cm^{-1} in PM and crystal in H_2O. The band which appears at 1643 cm^{-1} in the spectrum of the crystal is due to noise caused by the strong background absorption of the amide I and the bending mode of water. The TR spectra of other intermediates and spectra of L recorded at cryotemperature (data not shown) clearly show C=N stretching vibrations of SB at 1639 cm^{-1} in crystal. An important feature of the L intermediate is the negative band at 1740 cm^{-1}, which has been assigned to shifts in the frequencies of the carbonyl stretching vibrations of protonated Asp-96 and Asp-115 (41–43).

The second spectra (Fig. 6 *b*) are also very similar for PM and crystal. These spectra are representative for the M to ground state difference as the negative intensity at ~1186 cm^{-1} is indicative for the deprotonated SB (38,40). The positive band at ~1760 cm^{-1} has been assigned to the C=O stretch of Asp-85. It peaks at 1760 for the crystal and at 1762 cm^{-1} for PM (see also supplemental Fig. S1). The high frequencies together with the absence of an intense negative band at 1670 cm^{-1} indicate that admixtures from the N state are negligible in the spectra. The broad positive band centered around 1560 cm^{-1} is a mixture of the ethylenic vibration of the retinal at 1566 cm^{-1} (36), a C-N stretching vibration of Arg-82 (44), and the amide II vibration of the protein backbone (40). The positive band at 1619 cm^{-1} indicates the C=N stretch of the SB in the M state (45) and changes in amide I vibrations of Lys-216 (46).

Unlike the first two difference spectra, the third one of the bR crystal deviates considerably from that of PM (Fig. 6 *c*). In the case of PM, the carbonyl vibration of Asp-85 absorbs at 1760 cm^{-1} and is broader than in the M state due to an increase in absorbance at ~1755 cm^{-1} (supplementary information I). The positive absorbance at 1186 cm^{-1} indicates a mixture of intermediates with a protonated SB, i.e., N and O states. Among them, the O state is dominant as judged by the appearance of the characteristic C=C stretch at 1506 cm^{-1}, whereas small bands at 1670 and 1553 cm^{-1} (Fig. 7) indicate minor contributions from the N state (38,47). This is in agreement with UV/Vis time-resolved measurements (Fig. 3) and with the fact that the N state is not accumulated to high transient concentration at pH 5.6 (the concentration of the N state titrates with an apparent pK_a of ~7 (48)).

The third difference spectrum of the bR crystal shows that major contributions result from the N state. However an essential fraction of the M state is still present. The following bands are marker bands for the N state (40,47): The carbonyl vibration of Asp-85 absorbs maximally at 1756 cm^{-1}, a pronounced negative amide I band appears at 1670 cm^{-1}, a positive amide II band at 1554 cm^{-1}, and a positive C-C stretching vibration of retinal at 1186 cm^{-1}. The absence of a band at 1506 cm^{-1} indicates that the O state does not contribute to the spectrum, which agrees with the results from time-resolved UV/Vis spectroscopy (Fig. 3). Deprotonation of Asp-96 is indicated by the negative absorbance at 1741cm^{-1} (41). This weak negative band appears late in the photocycle concomitantly with reprotonation of the SB (1186 cm^{-1}), as one can deduce from the respective kinetic traces in Fig. 7.

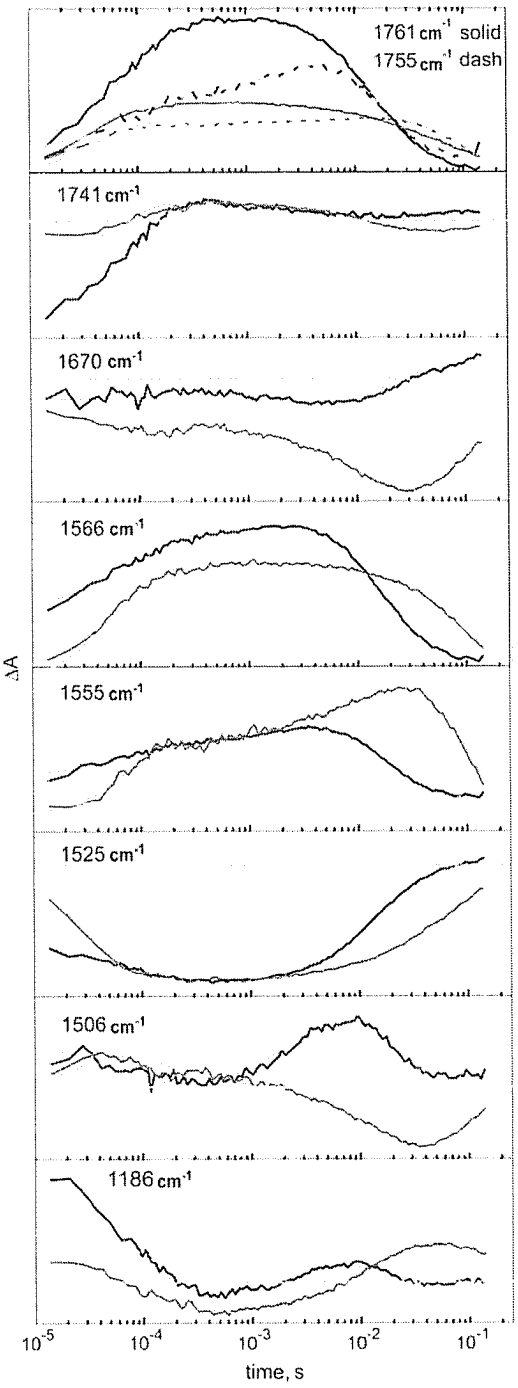

FIGURE 7 IR transients of the photoreaction of bR at characteristic frequencies. The black traces correspond to experiments on PM and the red traces to the single crystal. The smooth gray traces are due to the global fit with the sum of three exponentials. The horizontal dashed lines indicate the zero level of absorbance changes.

TR-FTIR in D_2O

TR experiments have been performed in D_2O for two reasons. From an IR spectroscopic view, the exchange of H_2O to D_2O removes the strong background absorption of the solvent, particularly in the diagnostic amide I region to gauge conformational changes of the protein backbone in the crystal. Additionally, bR exhibits characteristic KIEs when the protons are replaced by the heavier deuterons, which provides an additional measure for the functionality of the protein. The TR data were fitted with the sum of three exponentials likewise to the analysis of the data recorded in H_2O. The resulting time constants of the photocycle are 170 μs, 20 ms, and 84 ms for the bR crystal and 420 μs, 8.4 ms, and 14 ms for PM. The corresponding spectra are depicted in Fig. 8.

The spectrum corresponding to the shortest time constant represents the L to ground state difference spectrum (Fig. 8 *a*). Carbon-carbon vibrations of retinal are not influenced by the presence of D_2O (except for 1254 cm^{-1} coupled with in-plane bending vibration of SB N-H). The ethylenic stretching vibration of retinal is at 1526 cm^{-1} in the ground state and 1548 cm^{-1} in L, whereas the C-C stretching vibration absorbs at 1201 cm^{-1} and 1169 cm^{-1} in ground state bR and at 1190 cm^{-1} in L. The negative band at 1728 with a shoulder at 1734 cm^{-1} observed in PM and crystal are assigned to alterations in hydrogen-bonding of Asp-115 and Asp-96, respectively (41). In addition to this band, a small positive band at 1751 cm^{-1} is observed in the spectrum of crystal due to a minor contribution of the M state (see Fig. S2 in the Supplementary Material). The C=N stretching vibration of the SB is found at 1624 and 1626 cm^{-1} for PM and crystal, respectively. Isotopic substitution prolongs the lifetime of the L state, which agrees with the TR UV/Vis measurements (Fig. 4). In D_2O the L state decays 2.4 times faster in the crystal than in PM (Fig. 9).

The second difference spectra (Fig. 8 *b*) correspond to a nearly pure M state and agree well between PM and crystal.

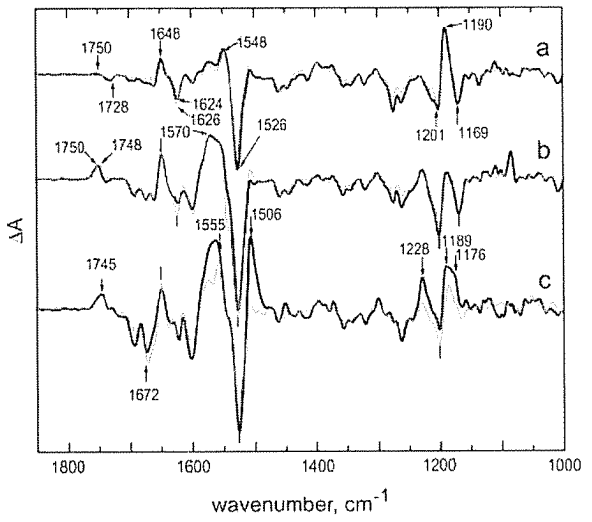

FIGURE 8 Difference spectra of the bR intermediates measured in D_2O at 20°C. The spectra have been obtained by fitting the photocycle kinetics with the sum of three exponentials. Black spectra correspond to the decay-associated difference spectra of bR in PM at time constants of 420 μs (*a*), 8.4 ms (*b*), and 14 ms (*c*). Spectra in red are the decay-associated difference spectra of bR in the single 3D crystal at time constants of 170 μs (*a*), 20 ms (*b*), and 84 ms (*c*).

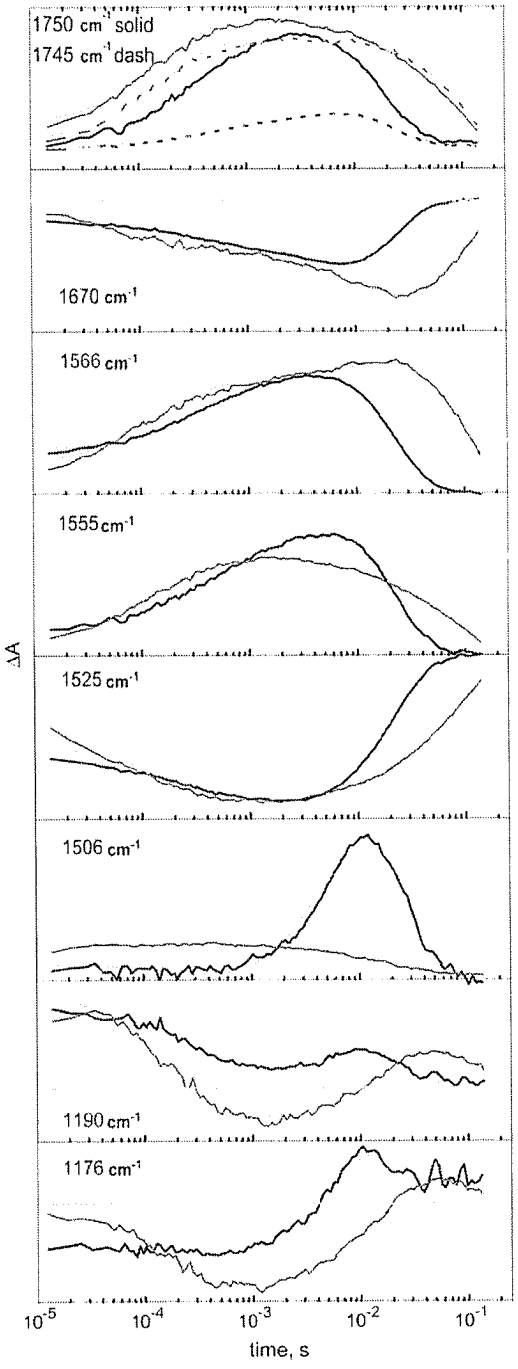

FIGURE 9 TR photocycle kinetics of bR in PM (*black traces*) and in the single crystal (*red traces*) in D_2O are shown for characteristic bands. The gray traces correspond to the global fit.

Deprotonation of the SB is deducible from the negative intensity at 1190 cm^{-1}. The protonation of Asp-85 is indicated by a positive band at 1750 and 1748 cm^{-1} in PM and crystal, respectively (Fig. S2, (37,49)). The broad positive band at ~1560 cm^{-1} is composed of nearly equally intense bands of the ethylenic stretching vibration of retinal at 1570 cm^{-1} (37) and the amide II band at 1554 cm^{-1}. A positive band at 1648 cm^{-1} has been assigned to amide I vibrations of the protein (37,50). These features comprise a fingerprint of the M state.

In the spectra corresponding to the slowest time constant, the carbonyl band of Asp-85 is asymmetric, with maximum at 1745 and a shoulder at 1750 cm^{-1} in PM and crystal (Figs. 8 *c* and S2). This indicates that the spectra contain an essential fraction of the M intermediate, dominated by the later intermediates of the photocycle. In PM, these intermediates are the N and O states. The bands at 1672(−), 1555(+), 1228(+), and 1189 cm^{-1} are characteristic of the N intermediate, whereas those at 1730(+), 1506(+), and 1176(+) characterize the O intermediate (38). These intermediates appear nearly synchronously in the photocycle of PM as is obvious from the time traces at characteristic wavenumbers (Fig. 9). Therefore, they are represented by one difference spectrum in the sequential unidirectional model applied here.

In the spectrum of the crystal, the characteristic bands at 1555 and 1672 cm^{-1} clearly demonstrate the occurrence of protein conformational changes, typical for the N state (Fig. 9). No substantial accumulation of the O state is observed in the crystal as obvious from the difference absorbance trace at 1506 cm^{-1} (Fig. 9).

The KIE on the late part of the photocycle is small, which agrees with the results from TR UV-Vis experiments.

DISCUSSION

This spectroscopic study of the photoinduced kinetics of a single bR crystal aimed to characterize the putative influence of the crystal lattice on the dynamics of the protein. Since our results agree well with the huge number of spectroscopic data that were recorded on PM, we can correlate the single crystal kinetics to the multiple crystallographic structures obtained for ground state bR and the photocycle intermediates.

Ground state structure

We have observed that the UV-Vis absorbance spectra of PM and crystal are identical (Fig. 2). The frequencies of the retinal vibrations, which are extremely sensitive markers for the conformation of the chromophore (51,52), are also not influenced by the crystalline packing (Figs. 5 and 6). In particular, the C=N stretching vibration of the retinal SB, which critically depends on hydrogen-bonding interaction with its immediate vicinity, is the same in the crystal as in the native PM. These observations imply that the structure of retinal and its binding pocket is the same for bR in the 3D crystal and in the native membrane. Schenkl et al. (15) have concluded from UV/Vis absorption and fluorescence spectroscopy that bR crystals embedded in the lipidic cubic phase are strongly dehydrated. We have also observed a dramatic deceleration of the photocycle upon partial dehydration of the crystal (data not shown). The effect is induced even at short exposure (~1 min) of the well-hydrated crystal to room atmosphere. In contrast to the work by Schenkl et al. (15), we isolated single bR crystals from the cubic phase and immersed them in aqueous buffer solution. Under these conditions neither the visible absorbance spectrum nor the FTIR difference spectrum (see below) reveal signs of essential dehydration of the bR crystal, which would suppress bR functionality. Moreover, the observation of an appreciable KIE on the photocycle and isotopic shifts of specific FTIR bands suggests that the solvent can diffuse into the bR crystals. This is in line with the earlier observed ion exchange in bR crystals of space group $C222_1$ grown in cubo (53).

Light/dark adaptation as monitored by steady-state FTIR difference spectroscopy did not reveal any deviation between the crystal and PM. This observation suggests that the retinal conformation is not disturbed by the crystalline packing of the bR molecules. Special care should be taken in crystallographic experiments to ensure complete light adaptation, particularly in the case of thick crystals. This is of particular importance for the structure determination of intermediate states as the conformation of dark-adapted bR is difficult to disentangle from the respective photocycle intermediate. Thus, the significance of the structure of the latter is blurred.

In this context, it is worthwhile to compare the molecular structure of the retinal binding pocket of bR as solved from 3D crystals by x-ray crystallography (10) with electron microscopic structures from PM (54,55). The root mean square deviations of the coordinates of those amino acids within 5-Å distance from retinal are all within the experimental error of 1 Å. This corroborates the conclusions from our spectroscopic results.

Proton transfer dynamics

The dynamics of proton transfer within the crystal is of crucial importance as it refers to the functionality of bR. TR FTIR measurements show that SB deprotonates and Asp-85 protonates in the crystal upon formation of the M state. The frequency of the C=O stretch of the proton acceptor Asp-85 is 2 cm^{-1} lower in the crystal than in PM. This holds true not only for H_2O and D_2O as solvent (Figs. 6 *b* and 8 *b*) but also at low temperatures (data not shown). Hence, the environment of Asp-85 in crystal is more hydrophilic (or H-bonding is stronger) than in PM, and its pK_a is higher. In the millisecond range after photoexcitation, the carbonyl stretching vibration of protonated Asp-85 is downshifted from 1760 to 1755 cm^{-1} (47,56) in the crystal as well as in PM (Figs. 7 and 9). This frequency shift has been correlated to a pK_a increase of Asp-85 by ~0.5 (40). On the same timescale, the SB is reprotonated (1186(+) cm^{-1}) and the negative band

at 1741 cm^{-1} indicates the deprotonation of Asp-96 (Fig. 7). These observations suggest that the reprotonation of the SB occurs from the cytoplasmic side. Since the major steps characteristic for proton translocation are observed in the crystal, we conclude that crystalline bR pumps protons.

Conformational changes

It is known that the capacity of bR to perform structural changes depends critically on the water content (57,58). It was shown by FTIR spectroscopy that the amplitude of the conformational changes starts to diminish at 70% (w/v) water concentration and completely vanishes at 25% (50). It is known that the N state can be accumulated only when PM is highly hydrated (12,47). It is striking though that in the crystals containing just ~20% water by volume (9), bR does not exhibit signs of strong dehydration: Conformational changes do occur in the photocycle, and the N state accumulates to an even higher extent than in PM. Thus, we conclude that the low water content in the crystal does not impair the protein's functionality.

Kinetics

We have observed that the kinetics of the photocycle in the crystal is noticeably different from that of PM. The M state rises faster and lives longer in the crystal than in PM under identical conditions. The accumulation of the O state is hampered in the crystal whereas N is favored. The KIE of H^+ transfer is similar in the crystal and PM.

Among the relevant factors known to alter photocycle kinetics are water content (50,57,58) and lipid composition (59–61). Thin water layers that separate the two adjacent bR layers are ~10-Å thick in the 3D crystal. Thus, the apparent dielectric permittivity is different from that of bulk water. Consequently, alterations to the protein surface electrostatics are induced which may influence the photocycle kinetics.

Change in lipid content is another plausible reason for kinetic alterations. Indeed, the available high-resolution structures of bR provide evidence for endogenous lipids in the crystal (10,62). However, these studies were unable to quantify the lipid composition. Qualitatively, a difference in lipid content is indicated by a reduced in-plane lattice constant: 60.8 ± 0.1 Å of crystal (10,62,63) versus 61.2 ± 0.1 Å for PM (64). Matrix-assisted laser desorption ionization experiments on bR crystals suggest the lack of two different endogenous lipids (62). Such a partial delipidation accelerates the rise of the M state and decelerates its decay in PM (59), similar to what is observed in the crystal.

In the crystal, we observe a 2-cm^{-1} downshift of the frequency of the carbonyl stretching vibration of (protonated) Asp-85 in the M state. It was earlier suggested that such a shift correlates with the pK_a of the proton release group (48). Thus, proton release by bR is delayed in PM, whereas it is accelerated in the crystal under the conditions used in this work (3 M phosphate, pH 5.6). Hence, either the structure of the proton release complex is altered in the crystal as compared to PM, or the local electrostatics in its immediate environment is different. Both changes might be evoked by the absence of particular polar lipids in the crystal.

Implications for the nature of the trapped intermediate states used in x-ray crystallography

The structural model of the L state is currently the most controversial (65). As the transitions from one state to another are thermally driven, our observation of the faster kinetics of the L decay in the crystal implies that it is less stable at low temperature than the L state in PM. Indeed, it was observed that the L state is accumulated at temperatures not higher than 150 K in the crystal, which is 20 K lower than in PM (13,14,65). The accelerated decay of the L state is in line with an increased pK_a of Asp-85, since it would facilitate protonation of the residue in the crystal as compared to PM.

Another intermediate that is affected by the difference in kinetics is the N state. Our data on the photocycle kinetics in the crystal allow an independent assignment of the intermediate trapped by illumination of the crystal at room temperature and after flash cooling (66). It follows from the photocycle kinetics and supported by steady-state FTIR measurements (data not shown) that a mixture of M and N states with high occupancies accumulates under steady-state illumination. Subsequent flash cooling results in higher population of the M state. This agrees with an assignment based on comparison of low-resolution projection maps calculated from the structure of crystal intermediate with experimental maps for PM (67). Hence, it is due to the photocycle kinetics specific for the crystal that the N state can be trapped by flash cooling under constant illumination.

The last intermediate of the photocycle, the O state, is difficult to accumulate at ambient temperatures (38) and not possible to trap at low temperature in PM. Moreover, it is even more difficult in the crystal (Fig. 4). Thus, the O state of wild-type bR remains a challenge for high-resolution crystallographic structural studies.

SUPPLEMENTARY MATERIAL

An online supplement to this article can be found by visiting BJ Online at http://www.biophysj.org.

We thank C. Baeken for excellent technical assistance and M. Liatti and S. Lehmann for help in construction of the flash-photolysis apparatus.

This work was supported by the Alexander von Humboldt Foundation.

REFERENCES

1. Oesterhelt, D., and W. Stoeckenius. 1973. Functions of a new photoreceptor membrane. *Proc. Natl. Acad. Sci. USA.* 70:2853–2857.
2. Lanyi, J. K. 2004. Bacteriorhodopsin. *Annu. Rev. Physiol.* 66:665–688.

3. Oesterhelt, D. 1998. The structure and mechanism of the family of retinal proteins from halophilic archaea. *Curr. Opin. Struct. Biol.* 8: 489–500.

4. Landau, E. M., and J. P. Rosenbusch. 1996. Lipidic cubic phases: a novel concept for the crystallization of membrane proteins. *Proc. Natl. Acad. Sci. USA.* 93:14532–14535.

5. Faham, S., and J. U. Bowie. 2002. Bicelle crystallization: a new method for crystallizing membrane proteins yields a monomeric bacteriorhodopsin structure. *J. Mol. Biol.* 316:1–6.

6. Essen, L. O., R. Siegert, W. D. Lehmannn, and D. Oesterhelt. 1998. Lipid patches in membrane protein oligomers: crystal structure of the bacteriorhodopsin-lipid complex. *Proc. Natl. Acad. Sci. USA.* 95: 11673–11678.

7. Takeda, K., H. Sato, T. Hino, M. Kono, K. Fukuda, I. Sakurai, T. Okada, and T. Kouyama. 1998. A novel three-dimensional crystal of bacteriorhodopsin obtained by successive fusion of the vesicular assemblies. *J. Mol. Biol.* 283:463–474.

8. Lanyi, J. K., and B. Schobert. 2004. Local-global conformational coupling in a heptahelical membrane protein: transport mechanism from crystal structures of the nine states in the bacteriorhodopsin photocycle. *Biochemistry.* 43:3–8.

9. Pebay-Peyroula, E., G. Rummel, J. P. Rosenbusch, and E. M. Landau. 1997. X-ray structure of bacteriorhodopsin at 2.5 angstroms from microcrystals grown in lipidic cubic phases. *Science.* 277:1676–1681.

10. Luecke, H., B. Schobert, H. T. Richter, J. P. Cartailler, and J. K. Lanyi. 1999. Structure of bacteriorhodopsin at 1.55 Å resolution. *J. Mol. Biol.* 291:899–911.

11. Heberle, J., G. Büldt, E. Koglin, J. P. Rosenbusch, and E. M. Landau. 1998. Assessing the functionality of a membrane protein in a three-dimensional crystal. *J. Mol. Biol.* 281:587–592.

12. Balashov, S. P., and T. G. Ebrey. 2001. Trapping and spectroscopic identification of the photointermediates of bacteriorhodopsin at low temperatures. *Photochem. Photobiol.* 73:453–462.

13. Lanyi, J. K., and B. Schobert. 2003. Mechanism of proton transport in bacteriorhodopsin from crystallographic structures of the K, L, M-1, M-2, and M-2′ intermediates of the photocycle. *J. Mol. Biol.* 328: 439–450.

14. Royant, A., K. Edman, T. Ursby, E. Pebay-Peyroula, E. M. Landau, and R. Neutze. 2001. Spectroscopic characterization of bacteriorhodopsin's L-intermediate in 3D crystals cooled to 170 K. *Photochem. Photobiol.* 74:794–804.

15. Schenkl, S., E. Portuondo, G. Zgrablic, M. Chergui, W. Suske, M. Dolder, E. M. Landau, and S. Haacke. 2003. Compositional heterogeneity reflects partial dehydration in three-dimensional crystals of bacteriorhodopsin. *J. Mol. Biol.* 329:711–719.

16. Edman, K., P. Nollert, A. Royant, H. Belrhali, E. Pebay-Peyroula, J. Hajdu, R. Neutze, and E. M. Landau. 1999. High-resolution x-ray structure of an early intermediate in the bacteriorhodopsin photocycle. *Nature.* 401:822–826.

17. Lanyi, J., and B. Schobert. 2002. Crystallographic structure of the retinal and the protein after deprotonation of the Schiff base: the switch in the bacteriorhodopsin photocycle. *J. Mol. Biol.* 321:727–737.

18. Fedorov, R., I. Schlichting, E. Hartmann, T. Domratcheva, M. Fuhrmann, and P. Hegemann. 2003. Crystal structures and molecular mechanism of a light-induced signaling switch: the Phot-LOV1 domain from *Chlamydomonas reinhardtii*. *Biophys. J.* 84:2474–2482.

19. Kort, R., R. B. Ravelli, F. Schotte, D. Bourgeois, W. Crielaard, K. J. Hellingwerf, and M. Wulff. 2003. Characterization of photocycle intermediates in crystalline photoactive yellow protein. *Photochem. Photobiol.* 78:131–137.

20. Schobert, B., L. S. Brown, and J. K. Lanyi. 2003. Crystallographic structures of the M and N intermediates of bacteriorhodopsin: assembly of a hydrogen-bonded chain of water molecules between Asp-96 and the retinal Schiff base. *J. Mol. Biol.* 330:553–570.

21. Ng, K., E. D. Getzoff, and K. Moffat. 1995. Optical studies of a bacterial photoreceptor protein, photoactive yellow protein, in single crystals. *Biochemistry.* 34:879–890.

22. Gerwert, K., B. Hess, H. Michel, and S. Buchanan. 1988. FTIR studies on crystals of photosynthetic reaction centers. *FEBS Lett.* 232:303–307.

23. Facciotti, M. T., S. Rouhani, F. T. Burkard, F. M. Betancourt, K. H. Downing, R. B. Rose, G. McDermott, and R. M. Glaeser. 2001. Structure of an early intermediate in the M-state phase of the bacteriorhodopsin photocycle. *Biophys. J.* 81:3442–3455.

24. Oesterhelt, D., and W. Stoeckenius. 1974. Isolation of the cell membrane of Halobacterium halobium and its fractionation into red and purple membrane. *Methods Enzymol.* 31:667–686.

25. Gordeliy, V. I., R. Schlesinger, R. Efremov, G. Büldt, and J. Heberle. 2003. Crystallization in lipidic cubic phases: a case study with bacteriorhodopsin. *In* Membrane Protein Protocols: Expression, Purification, and Crystallization. B. Selinsky, editor. Humana Press, Totowa, NJ. 305–316.

26. Muller, K. H., and T. Plesser. 1991. Variance reduction by simultaneous multiexponential analysis of data sets from different experiments. *Eur. Biophys. J.* 19:231–240.

27. Chizhov, I., D. S. Chernavskii, M. Engelhard, K. H. Mueller, B. V. Zubov, and B. Hess. 1996. Spectrally silent transitions in the bacteriorhodopsin photocycle. *Biophys. J.* 71:2329–2345.

28. Fischer, U., and D. Oesterhelt. 1979. Chromophore equilibria in bacteriorhodopsin. *Biophys. J.* 28:211–230.

29. Dencher, N. A., and M. P. Heyn. 1978. Formation and properties of bacteriorhodopsin monomers in the non-ionic detergents octyl-beta-D-glucoside and Triton X-100. *FEBS Lett.* 96:322–326.

30. Metz, G., F. Siebert, and M. Engelhard. 1992. Asp85 is the only internal aspartic acid that gets protonated in the M intermediate and the purple-to-blue transition of bacteriorhodopsin. A solid-state 13C CP-MAS NMR investigation. *FEBS Lett.* 303:237–241.

31. Hildebrandt, P., and M. Stockburger. 1984. Role of water in bacteriorhodopsin's chromophore: resonance Raman study. *Biochemistry.* 23:5539–5548.

32. le Coutre, J., and K. Gerwert. 1996. Kinetic isotope effects reveal an ice-like and a liquid-phase-type intramolecular proton transfer in bacteriorhodopsin. *FEBS Lett.* 398:333–336.

33. Balashov, S. P., M. Lu, E. S. Imasheva, R. Govindjee, T. G. Ebrey, B. Othersen, Y. M. Chen, R. K. Crouch, and D. R. Menick. 1999. The proton release group of bacteriorhodopsin controls the rate of the final step of its photocycle at low pH. *Biochemistry.* 38:2026–2039.

34. Pettei, M. J., A. P. Yudd, K. Nakanishi, R. Henselman, and W. Stoeckenius. 1977. Identification of retinal isomers isolated from bacteriorhodopsin. *Biochemistry.* 16:1955–1959.

35. Scherrer, P., M. K. Mathew, W. Sperling, and W. Stoeckenius. 1989. Retinal isomer ratio in dark-adapted purple membrane and bacteriorhodopsin monomers. *Biochemistry.* 28:829–834.

36. Maeda, A. 1995. Application of FTIR spectroscopy to the structural study on the function of bacteriorhodopsin. *Isr. J. Chem.* 35:387–400.

37. Bagley, K., G. Dollinger, L. Eisenstein, A. K. Singh, and L. Zimanyi. 1982. Fourier transform infrared difference spectroscopy of bacteriorhodopsin and its photoproducts. *Proc. Natl. Acad. Sci. USA.* 79: 4972–4976.

38. Zscherp, C., and J. Heberle. 1997. Infrared difference spectra of the intermediates L, M, N, and O of the bacteriorhodopsin photoreaction obtained by time-resolved attenuated total reflection spectroscopy. *J. Phys. Chem. B.* 101:10542–10547.

39. Hessling, B., G. Souvignier, and K. Gerwert. 1993. A model-independent approach to assigning bacteriorhodopsin's intramolecular reactions to photocycle intermediates. *Biophys. J.* 65:1929–1941.

40. Braiman, M. S., O. Bousche, and K. J. Rothschild. 1991. Protein dynamics in the bacteriorhodopsin photocycle: submillisecond Fourier transform infrared spectra of the L, M, and N photointermediates. *Proc. Natl. Acad. Sci. USA.* 88:2388–2392.

41. Maeda, A., J. Sasaki, Y. Shichida, T. Yoshizawa, M. Chang, B. Ni, R. Needleman, and J. K. Lanyi. 1992. Structures of aspartic acid-96 in the L and N intermediates of bacteriorhodopsin: analysis by Fourier transform infrared spectroscopy. *Biochemistry.* 31:4684–4690.

42. Gerwert, K., B. Hess, J. Soppa, and D. Oesterhelt. 1989. Role of aspartate-96 in proton translocation by bacteriorhodopsin. *Proc. Natl Acad. Sci. USA.* 86:4943–4947.

43. Braiman, M. S., T. Mogi, T. Marti, L. J. Stern, H. G. Khorana, and K. J. Rothschild. 1988. Vibrational spectroscopy of bacteriorhodopsin mutants: light-driven proton transport involves protonation changes of aspartic acid residues 85, 96, and 212. *Biochemistry.* 27:8516–8520.

44. Hutson, M. S., U. Alexiev, S. V. Shilov, K. J. Wise, and M. S. Braiman. 2000. Evidence for a perturbation of arginine-82 in the bacteriorhodopsin photocycle from time-resolved infrared spectra. *Biochemistry.* 39:13189–13200.

45. Lewis, A., J. Spoonhower, R. A. Bogomolni, R. H. Lozier, and W. Stoeckenius. 1974. Tunable laser resonance Raman spectroscopy of bacteriorhodopsin. *Proc. Natl Acad. Sci. USA.* 71:4462–4466.

46. Takei, H., Y. Gat, Z. Rothman, A. Lewis, and M. Sheves. 1994. Active site lysine backbone undergoes conformational changes in the bacteriorhodopsin photocycle. *J. Biol. Chem.* 269:7387–7389.

47. Pfefferle, J. M., A. Maeda, J. Sasaki, and T. Yoshizawa. 1991. Fourier transform infrared study of the N intermediate of bacteriorhodopsin. *Biochemistry.* 30:6548–6556.

48. Zscherp, C., R. Schlesinger, J. Tittor, D. Oesterhelt, and J. Heberle. 1999. *In situ* determination of transient pKa changes of internal amino acids of bacteriorhodopsin by using time-resolved attenuated total reflection Fourier-transform infrared spectroscopy. *Proc. Natl. Acad. Sci. USA.* 96:5498–5503.

49. Engelhard, M., K. Gerwert, B. Hess, W. Kreutz, and F. Siebert. 1985. Light-driven protonation changes of internal aspartic acids of bacteriorhodopsin: an investigation by static and time-resolved infrared difference spectroscopy using [4–13C]aspartic acid labeled purple membrane. *Biochemistry.* 24:400–407.

50. Braiman, M. S., P. L. Ahl, and K. J. Rothschild. 1987. Millisecond Fourier-transform infrared difference spectra of bacteriorhodopsin's M412 photoproduct. *Proc. Natl Acad. Sci. USA.* 84:5221–5225.

51. Smith, S. O., J. Lugtenburg, and R. A. Mathies. 1985. Determination of retinal chromophore structure in bacteriorhodopsin with resonance Raman spectroscopy. *J. Membr. Biol.* 85:95–109.

52. Althaus, T., W. Eisfeld, R. Lohrmann, and M. Stockburger. 1995. Application of Raman spectroscopy to retinal proteins. *Isr. J. Chem.* 35:227–251.

53. Facciotti, M. T., V. S. Cheung, D. Nguyen, S. Rouhani, and R. M. Glaeser. 2003. Crystal structure of the bromide-bound D85S mutant of bacteriorhodopsin: principles of ion pumping. *Biophys. J.* 85:451–458.

54. Mitsuoka, K., T. Hirai, K. Murata, A. Miyazawa, A. Kidera, Y. Kimura, and Y. Fujiyoshi. 1999. The structure of bacteriorhodopsin at 3.0 Å resolution based on electron crystallography: implication of the charge distribution. *J. Mol. Biol.* 286:861–882.

55. Subramaniam, S., and R. Henderson. 2000. Molecular mechanism of vectorial proton translocation by bacteriorhodopsin. *Nature.* 406: 653–657.

56. Sasaki, J., Y. Shichida, J. K. Lanyi, and A. Maeda. 1992. Protein changes associated with reprotonation of the Schiff base in the photocycle of Asp96→Asn bacteriorhodopsin. The MN intermediate with unprotonated Schiff base but N-like protein structure. *J. Biol. Chem.* 267:20782–20786.

57. Dencher, N. A., H. J. Sass, and G. Büldt. 2000. Water and bacteriorhodopsin: structure, dynamics, and function. *Biochim. Biophys. Acta.* 1460:192–203.

58. Sass, H. J., I. W. Schachowa, G. Rapp, M. H. Koch, D. Oesterhelt, N. A. Dencher, and G. Büldt. 1997. The tertiary structural changes in bacteriorhodopsin occur between M states: x-ray diffraction and Fourier transform infrared spectroscopy. *EMBO J.* 16:1484–1491.

59. Fitter, J., S. A. Verclas, R. E. Lechner, H. Seelert, and N. A. Dencher. 1998. Function and picosecond dynamics of bacteriorhodopsin in purple membrane at different lipidation and hydration. *FEBS Lett.* 433:321–325.

60. Hildebrandt, V., K. Fendler, J. Heberle, A. Hoffmann, E. Bamberg, and G. Büldt. 1993. Bacteriorhodopsin expressed in Schizosaccharomyces pombe pumps protons through the plasma membrane. *Proc. Natl Acad. Sci. USA.* 90:3578–3582.

61. Dracheva, S., S. Bose, and R. W. Hendler. 1996. Chemical and functional studies on the importance of purple membrane lipids in bacteriorhodopsin photocycle behavior. *FEBS Lett.* 382:209–212.

62. Belrhali, H., P. Nollert, A. Royant, C. Menzel, J. P. Rosenbusch, E. M. Landau, and E. Pebay-Peyroula. 1999. Protein, lipid and water organization in bacteriorhodopsin crystals: a molecular view of the purple membrane at 1.9 Å resolution. *Struct. Fold. Des.* 7: 909–917.

63. Efremov, R., R. Moukhametzianov, G. Buldt, and V. Gordeliy. 2004. Physical detwinning of hemihedrally twinned hexagonal crystals of bacteriorhodopsin. *Biophys. J.* 87:3608–3613.

64. Zaccai, G. 1987. Structure and hydration of purple membranes in different conditions. *J. Mol. Biol.* 194:569–572.

65. Lanyi, J. K. 2004. What is the real crystallographic structure of the L photointermediate of bacteriorhodopsin? *Biochim. Biophys. Acta.* 1658:14–22.

66. Sass, H. J., G. Büldt, R. Gessenich, D. Hehn, D. Neff, R. Schlesinger, J. Berendzen, and P. Ormos. 2000. Structural alterations for proton translocation in the M state of wild-type bacteriorhodopsin. *Nature.* 406:649–653.

67. Kamikubo, H., and M. Kataoka. 2005. Can the low-resolution structures of photointermediates of bacteriorhodopsin explain their crystal structures? *Biophys. J.* 88:1925–1931.